Diamond to β-Sn phase transition of silicon under hydrostatic and nonhydrostatic compressions



2008 J. Phys.: Condens. Matter 20 325232

(http://iopscience.iop.org/0953-8984/20/32/325232)

J. Phys.: Condens. Matter **20** (2008) 325232 (6pp) doi:10.1088/0953-8984/20/32/325232

# Diamond to $\beta$-Sn phase transition of silicon under hydrostatic and nonhydrostatic compressions

**Murat Durandurdu**

Department of Physics, University of Texas at El Paso, El Paso, TX 79968, USA

Received 23 February 2008, in final form 26 June 2008
Published 18 July 2008
Online at stacks.iop.org/JPhysCM/20/325232

**Abstract**

We have carried out constant pressure *ab initio* simulations to study the pressure-induced phase transition of silicon. The diamond to $\beta$-Sn phase change under hydrostatic pressure is successfully observed in the simulation. The transformation is based on a fourfold coordinated tetragonal intermediate state having the space group $I4_1/amd$. The energy barrier for the transformation is calculated to be about 0.35 eV/atom. Additionally, we investigate the influence of nonhydrostatic compressions on the phase transition of silicon and find that up to 20% stress deviations, silicon converts to a $\beta$-Sn structure with a reduced transition pressure. The triaxial compressions cause more reduction in the transition pressure than the uniaxial compressions. The transformation mechanism is practically identical under both hydrostatic and nonhydrostatic conditions.

(Some figures in this article are in colour only in the electronic version)

## 1. Introduction

Silicon (Si) systems have a wide range of application in electronic and photoelectronic devices, and hence they have been studied extensively for decades. Yet new structures and properties are still being discovered. The high pressure phases of crystalline Si are well established: it shows 11 different solid structures between atmospheric pressure and 45 GPa. With the application of pressure, Si undergoes a first order phase transition from the diamond structure to the metallic $\beta$-Sn structure at approximately 12 GPa [1–3]. Under further compression, $\beta$-Sn transforms to the closely related $Imma$ phase at 13 GPa [4]. Near 16 GPa, the simple hexagonal (SH) state forms [2–4]. The hexagonal closed packed (HCP) structure is observed at 42 GPa [2, 3]. Additionally, a phase Si(VI) intermediated between SH and HCP has been obtained at 39 GPa [2]. Recently Si(VI) has been identified as an orthorhombic structure having 16 atoms per unit cell and space group symmetry $Cmca$ [5]. Upon release of pressure, Si does not transform back to the diamond structure. Instead the meta-stable BC8 phase is recovered on slow pressure release from $\beta$-Sn [6] while two tetragonal phases are obtained on very rapid pressure release [7].

These phase transformations have been successfully explained from the first principle calculations. However the methods have been mostly concerned with energy–volume calculations and the thermodynamic criterion of equal free energies [8, 9]. Recent developments have made it possible to observe directly the dynamical aspect of the solid–solid phase transitions with increasing pressure. Focher *et al* [10] employed a first principle constant pressure molecular dynamics (MD) technique within Parrinello–Rahman (PR) method [11] and found that Si directly transformed into the SH phase at 30 GPa. Morishita and Nosé obtained the same first order phase transition at 26 GPa using the PR method [12]. In a preliminary study, using an approximate *ab initio* technique, we also obtained the formation of a SH state at 29.5 GPa [13]. On the other hand, the diamond to $\beta$-Sn phase transformation was successfully observed in a MD simulation using the Tersoff potential at 64 GPa [14]. In another MD simulation using again the Tersoff potential, the diamond to $\beta$-Sn phase transition was reproduced at 60 GPa [15].

Although the high pressure phases of Si were successfully observed in these studies, the predicted critical pressures (the meta-stable phase transition pressure) in these direct MD simulations were much higher than the experimental and theoretical (the total energy–volume calculation) values of 7–16 GPa. These overestimated transition pressures imply a high intrinsic activation barrier for transforming one solid phase into another in simulations. With particular conditions such

 

as finite size of the simulation cell, the lack of any defect in the simulated structure, the timescale of simulations etc are considered, such an overestimated transition pressure is anticipated [10, 14, 15]. On the other hand, the thermodynamic theorem does not take into account the possible existence of such an activation barrier separating two structural phases.

These MD simulations provide substantial information about the diamond to $\beta$-Sn phase transformation of Si but its behavior under nonhydrostatic conditions is still unclear in spite of a few theoretical calculations that focus on the influence of the degree of hydrostaticity on the transition pressure and enthalpy barrier [16–18]. Indeed studying Si under nonhydrostatic compressions is more desirable to understand the pressure-induced phase transition better because pressure in the diamond anvil cell is not exactly hydrostatic. In this paper, we perform a constant pressure *ab initio* technique to shed some light on the pressure-induced phase transition of Si under hydrostatic and nonhydrostatic conditions. The diamond to $\beta$-Sn phase transition is successfully reproduced through a simulation with the application of hydrostatic pressure. The transformation is due to the orthorhombic modification of the simulation cell and based on a fourfold coordinated tetragonal intermediate state having the space group $I4_1/amd$. The activation enthalpy for this phase change is predicted to be about 0.35 eV/atom. Under nonhydrostatic compressions we also find the formation of a $\beta$-Sn structure, again up to 20% stress deviations. The transition pressure, as expected, is noticeably reduced by changing the degree of hydrostatic compression. Furthermore, we determine that the transformation mechanism is basically identical in both hydrostatic and nonhydrostatic conditions.

## 2. Computational method

We used the first-principles pseudopotentials method within the density-functional theory(DFT) and the local-density approximation using the Ceperley–Alder functional [19] for the exchange–correlation energy. The calculation was carried out with the *ab initio* program SIESTA [20] using a linear combination of atomic orbitals as the basis set, and a norm-conservative Troullier–Martins Pseudopotential [21]. A split-valence single-$\xi$ basis set was employed. A uniform mesh with a plane wave cut-off of 40 Ryd was used to represent the electron density, the local part of the pseudopotentials, and the Hartree and the exchange–correlation potential. The simulation cell consists of 64 atoms with periodic boundary conditions. We used $\Gamma$-point sampling for the Brillouin zone integration, which is reasonable for a simulation cell with 64 atoms since the energy difference between the 64 atom simulation cell with only $\Gamma$ point and the 8 atom unit cell with 108-**k** points (see below) is less than about 0.03 eV/atom. The MD simulations were performed using the NPE (constant number of atoms, constant pressure, and constant enthalpy) ensemble. The reason for choosing this ensemble is to remove the thermal fluctuation, which facilitates an easier examination of the structure during the phase transformation. Pressure was applied via the method of Parrinello and Rahman [11] and the structure is equilibrated with a period of 2000 time steps (each time step is one femtosecond (fs)) at each applied pressure. A fictitious cell mass 900 amu was found to be suitable for these simulations. We also used the power quenching technique during the MD simulations. In this technique, each velocity component is quenched individually. At each time step, if the force and velocity components have opposite sign, the velocity component is set equal to zero. All atoms or supercell velocities (for cell shape optimizations) are then allowed to accelerate at the next time step.

For the enthalpy calculations, we only considered the unit cell (8 atoms) for both diamond and $\beta$-Sn structures and the Brillouin zone integration was performed with an automatically generated $6\times6\times6$ $k$-point mesh for both phases following the convention of Monkhorst and Pack [22].

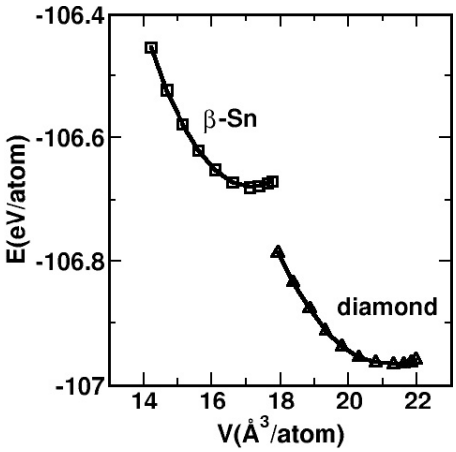


**Figure 1.** The energy volume curve of the diamond and $\beta$-Sn phases of Si.

## 3. Results

### *3.1. Enthalpy calculations*

We first consider the energy–volume calculations and the thermodynamic criterion of equal free energies to study the stability of the diamond and $\beta$-Sn phases of Si. These phases are equilibrated at several volumes and their energy–volume relations are fit to the third order Birch–Murnaghan equation of state. The computed total energy as a function of volume is given in figure 1. The relative energy difference between the diamond and $\beta$-Sn phases is 0.28 eV/atom, which is in agreement with previous DFT calculations of 0.27–0.28 eV/atom [23, 24].

The relative stability of the different phases of Si at finite pressure and temperature can be easily determined by a simple compression of their Gibbs free energies, $G = E_{\rm tot}+PV-TS$. Our DFT calculation is performed at zero temperature and hence the last term, entropic contribution, is neglected, which leads to the static enthalpy $H = E_{\rm tot} + PV$, where pressure is obtained by direct differentiation of the energy volume curves i.e., $P = -{\rm d}E_{\rm tot}/{\rm d}V$. In figure 2, we plot the computed enthalpy curve of the diamond and $\beta$-Sn phases as a function of pressure. The crossing of two curves indicates a phase transition between the two phases. The enthalpy curve of the

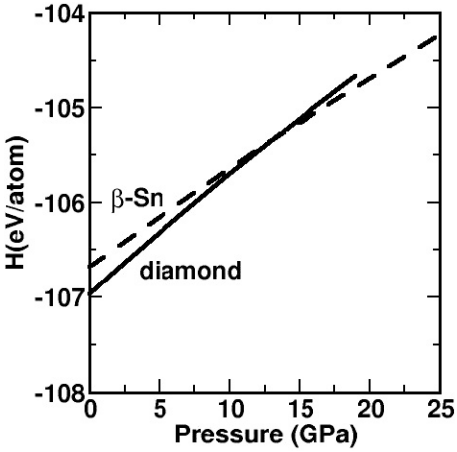


**Figure 2.** The calculated enthalpy of the diamond and $\beta$-Sn structures. The curves cross around 12.4 GPa, indicating a phase transition between the two phases.

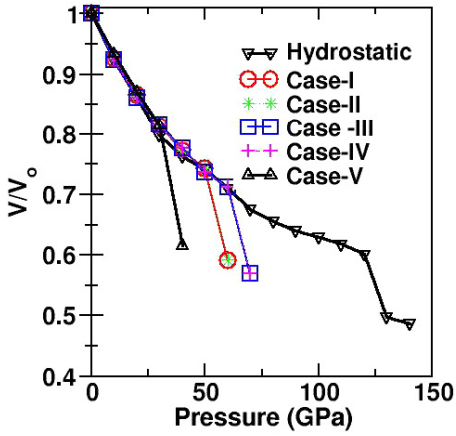


**Figure 3.** The pressure–volume curve of Si under hydrostatic and nonhydrostatic compressions from the dynamical simulations.

diamond phase crosses with that of the $\beta$-Sn phase around 12.4 GPa, in good agreement with about 7.0–19.0 GPa of the experimental observations [2, 3] and previous first-principles calculations [23–27].

From the energy–volume data, the bulk modulus of the diamond crystal is calculated to be 98.32 GPa, in excellent agreement with the experimental value of 99 GPa [28] and other theoretical values [23–27]. For the $\beta$-Sn phase, the bulk modulus is 123 GPa, which is again in good agreement with the previous first-principles result of 119 GPa [27]. The overall reasonable agreement for both transition parameters and bulk properties for Si with the experimental and theoretical results clearly reflects that the parameters used in the simulations are reliable and can also be applied to explore the pressure-induced phase transition of Si using constant pressure simulations.

### *3.2. Hydrostatic compression*

Figure 3 shows the pressure–volume relation obtained through the constant pressure simulation. Accordingly, the volume monotonically decreases with increasing pressure and the diamond structure is still preserved to 120 GPa. As the pressure is increased from 120 to 130 GPa, the structural phase transition begins and is accompanied by a sharp volume drop, which is a characteristic of a first order phase transition. Owing to the transformation, the diamond structure converts into a $\beta$-Sn structure as shown in figure 4, in agreement with experiments. Similar to the previous MD simulations [10, 12–15], the predicted transition pressure in the present study is considerably larger than the experimental results of 7–19 GPa. When particular conditions such as the use of a perfect structure, the size of the simulation etc are considered in the simulation, such a tendency is generally expected. Namely, since the simulated structure does not have any defect, the transformation does not proceed by nucleation and growth as seen in experiments, but instead it occurs across the entire simulation cell. Therefore, the system has to cross a high energy barrier to transform from one phase to another one and hence an overpressure is required to drive the phase transformation. This behavior is analogous to superheating in MD simulations. Of course, such a high critical pressure produces transformation parameters that cannot be comparable with experiments or enthalpy calculations that do not take into account the possible existence of such an activation barrier separating the two structural phases.

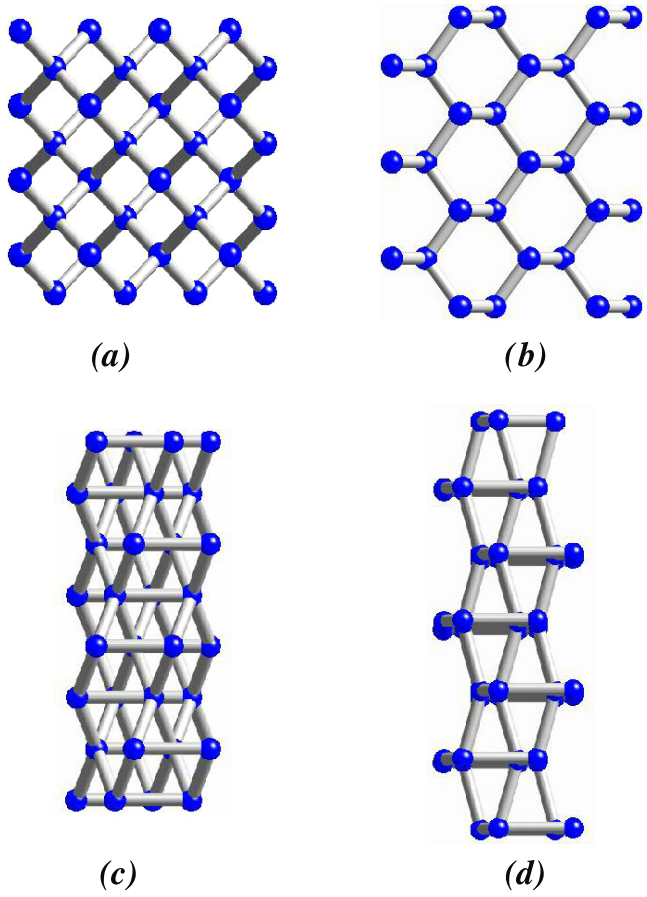


**Figure 4.** The diamond structure, viewed along (a) [001] and (b) [011]-directions. The $\beta$-Sn structure formed at 130 GPa under hydrostatic pressure, viewed along (c) [001] and (d) [011]-directions of the diamond structure.

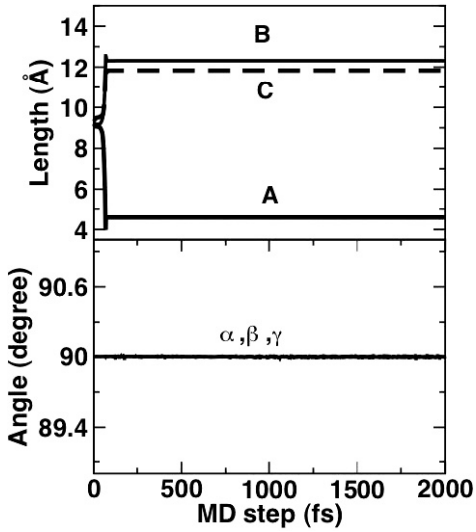


**Figure 5.** The time evolution of the simulation cell lengths and angles at 130 GPa under hydrostatic pressure.

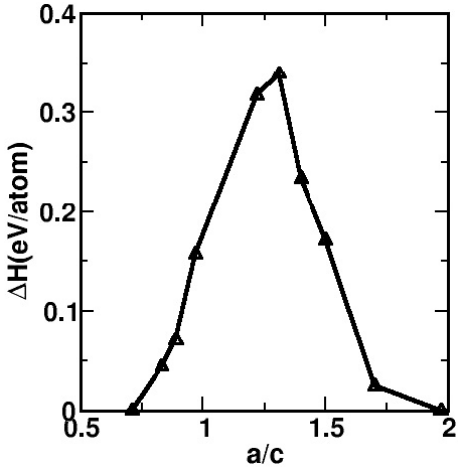


**Figure 6.** The minimum enthalpy barrier.

We next study the modification of the simulation cell to have a clear atomic level picture of the phase transformation. The variation of the simulation cell lengths and angles at 130.0 GPa as a function of MD time step is shown in figure 5. The simulation cell is initially oriented such that its lattice vectors **A**, **B**, and **C** are along the [100], [010] and [001] directions, respectively. The magnitude of these vectors is plotted in the figure. Accordingly, the simulation cell undergoes an orthorhombic distortion with a simultaneous expansion along the [010] and [001] directions and a contraction along the [100] direction and with no change in the simulation cell angles. The orthorhombic adaptation during the phase change is indeed different from our expectation of the tetragonal modification of the simulation cell, but a close analysis of the structure reveals that, in spite of the orthorhombic modification of the simulation cell (64 atoms), the unit cell of the structure during the phase change does indeed have a tetragonal symmetry and its lattice vectors are related to the simulation cell vectors by following relations: $\boldsymbol{a} = (\mathbf{B} - \mathbf{C})/4$, $\boldsymbol{b} = (\mathbf{B} + \mathbf{C})/4$, and $\boldsymbol{c} = \mathbf{A}/2$.

In order to see how the symmetry changes during the phase transformation, we analyze the structure each MD time step using the KPLOT program [29], which provides detailed information about space group, cell parameters and atomic positions of a given structure. For the symmetry analysis, we use 0.1 Å, 2°, and 0.7 Å tolerances for bond lengths, bond angles and interplanar spacing, respectively. At MD step 49, we successfully identify a fourfold coordinated tetragonal intermediate state within the $I4_1/amd$ symmetry. It should be noted here that the space group of this phase is the same as that of $\beta$-Sn. The lattice constant of this state is $a = b = 3.39$ Å and $c = 4.25$ Å. At later time steps, $a$ and $b$ gradually increase while $c$ decreases. At MD step 68, a sixfold coordinated $\beta$-Sn phase with the lattice parameters $a = b = 4.37$ Å and $c = 2.3$ Å forms. These results suggest that the phase transformation from diamond to the high pressure $\beta$-Sn structure can easily be pictured in terms of a tetragonal (along the principle axes) distortion of the unit cell. Although the transition is first order, there is an easy transition path that involves co-operative bond formation and lengthening, with no covalent bond breaking.

In previous classical MD simulations [14, 15] (but not quantum mechanical simulations [10, 11, 13]), the diamond to $\beta$-Sn phase transformation was successfully observed. In those studies [14, 15], during the phase transformation, two of the simulation cell lengths were expanded while the third one was contracted, similar to what we observe in the present study. The simulation cell lengths and angles, however, showed noticeable fluctuations, indicating small shear deformations during the phase transition and hence slight deviations from the ideal $\beta$-Sn structure [14, 15]. Therefore, the diamond to $\beta$-Sn phase transformation was associated with a monoclinic or triclinic modification of the simulation cell in the previous simulations, in a contrast to the orthorhombic adaption of the simulation cell in the present study, which produces a perfect $\beta$-Sn structure. In spite of these small discrepancies, the behavior of the simulation cell indicates that the transition mechanism observed in the previous simulations is practically similar to what has been observed in the present study.

We next calculate the activation enthalpy barrier of this simple phase transition. We prepare a series of intermediate structures that have $a/c$ ratios between the limiting values of 0.7 (diamond) and 1.96 ($\beta$-Sn). For each fixed $a/c$ ratio, we study the energy of these intermediate states as a function of volume and then calculate their enthalpy. Figure 6 shows the minimum enthalpy difference as a function of $a/c$ ratio at the static transition pressure of 12.4 GPa. Accordingly the enthalpy barrier between the two structures is about 0.35 eV/atom, which lies between the previously calculated first principles values of 0.2 eV/atom [14] and about 0.5 eV/atom [18] but close to 0.3 eV/atom [14] predicted using the Tersoff potential.

### *3.3. Nonhydrostatic compressions*

The degree of the hydrostaticity in experiments is determined by the efficiency of the pressure-transmitting medium. At

high pressures, the pressure-transmitting medium solidifies, resulting in strong nonhydrostatic effects. Even in the low pressure regime, pressure in the diamond anvil cell is not exactly hydrostatic. Consequently studying materials under nonhydrostatic conditions in simulations might be a more realistic approach to improving our understanding of their structural phase transitions and physical properties at high pressures. In this section, we investigate the influence of the degree of the hydrostatic compression on the phase transformation of Si using the Parrinello-Rahman and the power quenching techniques. We consider five different nonhydrostatic conditions and label them as case-I ($\sigma_x = 0.95P$, $\sigma_y = 0.9P$ and $\sigma_z = P$, where $P$ is the applied external pressure), case-II ($\sigma_x = 0.9P$, $\sigma_y = 0.95P$ and $\sigma_z = P$), case-III ($\sigma_x = 0.9P$, $\sigma_y = P$ and $\sigma_z = 0.9P$), case-IV ($\sigma_x = 0.9P$, $\sigma_y = 0.9P$ and $\sigma_z = P$) and case-V ($\sigma_x = 0.8P$, $\sigma_y = 0.9P$ and $\sigma_z = P$). The volume change under these loading conditions is represented in figure 3. Accordingly, Si shows practically identical equations of state under both hydrostatic and nonhydrostatic compressions but the critical pressure is notably reduced in the case of nonhydrostatic conditions (60 GPa for case-I and II, 70 GPa for case-III and IV and 40 GPa for case-V). For all cases studied, however, we find no indication of a new phase transformation in Si and instead the diamond structure converts into a $\beta$-Sn state. As expected, the transition volume (volume change) and the density of the final $\beta$-Sn phase are found to be sensitive to the transition pressure: as the transition pressure decreases, Si transforms into a more open $\beta$-Sn structure with a larger volume drop. When these cases are carefully analyzed, we see that the triaxial compressions (all stress components have different a value as in the case-I and II) cause more reduction in the transition pressure than the uniaxial stresses (two stress components have the same value while the third one has a different value as in the case-III and case-IV). This behavior might be explained by the tendency of the structure to adopt an orthorhombic modification during the phase transformation into $\beta$-Sn. Furthermore, although the nonhydrostatic compressions break the symmetry of the system even before the phase transition to $\beta$-Sn occurs (which is indeed the main reason for the reduced transition pressure), the mechanism obtained in these nonhydrostatic environments (see figures 7) is unexpectedly similar to what has been determined in the perfect hydrostatic condition. Therefore, we conclude that Si transforms into a $\beta$-Sn phase up to 20% deviation and the diamond to $\beta$-Sn transformation mechanism is independent of the degree of nonhydrostatic conditions in the simulations. However, we need to underline here that these conclusions are for the defect free silicon structure and such an ideal crystal might favor the formation of the $\beta$-Sn phase and produce an identical transformation path under both hydrostatic and nonhydrostatic conditions. In reality, phase transformations in experiments proceed by nucleation and growth at defects. Therefore, further studies are certainly needed to clearly understand the role of the stress deviations, defects, and their correlations on phase transformations.

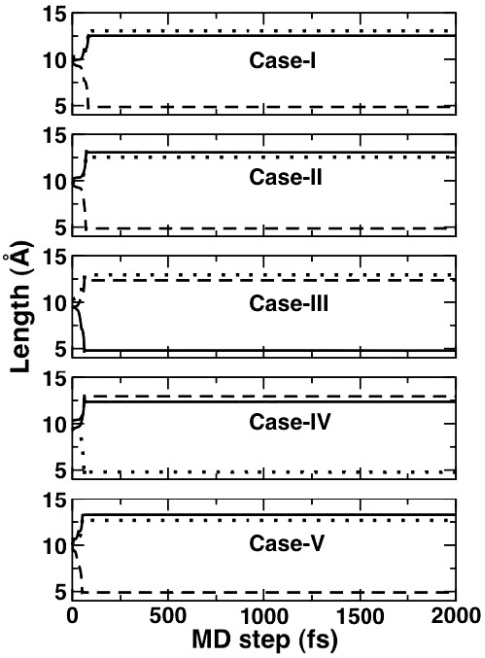


**Figure 7.** The time evolution of the simulation cell lengths under nonhydrostatic compressions.

## 4. Conclusions

We have studied the behavior of Si under both hydrostatic and nonhydrostatic compression. With the application of hydrostatic pressure, Si transforms into the $\beta$-Sn structure. The transformation is due to the orthorhombic modification of the simulation cell and is based on a fourfold coordinated tetragonal state. The energy barrier for the transformation is about 0.35 eV/atom. Under nonhydrostatic conditions, we also find the formation of the $\beta$-Sn phase up to 20% stress deviation, but the transition pressure is significantly reduced. Additionally it is found that the transformation mechanism under nonhydrostatic cases is similar to what has been determined under pure hydrostatic compression.

## Acknowledgment

The calculations were run on Sacagawea, a 128 processor Beowulf cluster, at the University of Texas at El Paso.

## References

[1] Gupta M C and Ruoff A L 1980 *J. Appl. Phys.* **51** 1072
[2] Olijnyk H, Sikka S K and Holzapfel W B 1987 *Phys. Lett.* A **103** 137
[3] Hu J Z, Merkle L D, Menoni C S and Spain I L 1986 *Phys. Rev.* B **34** 4679
Hu J Z and Spain I L 1984 *Solid State Commun.* **51** 263
[4] McMahon M I and Nelmes R J 1993 *Phys. Rev.* B **47** 8337
McMahon M I, Nelmes R J, Wright N G and Allan D R 1994 *Phys. Rev.* B **50** 739
[5] Hanfland M, Schwarz U, Syassen K and Takemura K 1999 *Phys. Rev. Lett.* **82** 1197

[6] Kasper S and Richards M S 1964 *Acta Crystallogr.* **17** 752
[7] Zhao Y X, Buehler F, Sites J R and Spain I L 1986 *Solid State Commun.* **59** 679
[8] Yin M T and Cohen M L 1980 *Phys. Rev. Lett.* **45** 1004
[9] Chang K J and Cohen M L 1985 *Phys. Rev.* B **31** 7819
[10] Focher P, Chiarotti G L, Bernasconi M, Tosatti E and Parrinello M 1994 *Europhys. Lett.* **26** 345
[11] Parrinello M and Rahman A 1980 *Phys. Rev. Lett.* **45** 1196
[12] Morishita T and Nosé S 2000 *Prog. Theor. Phys. Suppl.* **138** 251
[13] Durandurdu M and Drabold D A 2001 *Phys. Rev.* B **64** 014101
[14] Mizushima K, Yip S and Kaxiras E 1994 *Phys. Rev.* B **50** 14952
[15] Lee I H, Jeong J W and Chang K J 1997 *Phys. Rev.* B **55** 5689
[16] Cheng C, Huang W H and Li H J 2001 *Phys. Rev.* B **63** R153202
[17] Cheng C 2003 *Phys. Rev.* B **67** 134109
[18] Gaál-Nagy K and Strauch D 2006 *Phys. Rev.* B **73** 134101
[19] Ceperley D M and Alder M J 1980 *Phys. Rev. Lett.* **45** 566
[20] Ordejón P, Artacho E and Soler J M 1996 *Phys. Rev.* B **53** 10441
Sánchez-Portal D, Ordejón P, Artacho E and Soler J M 1997 *Int. J. Quantum Chem.* **65** 453
[21] Troullier N and Martins J L 1997 *Phys. Rev.* B **43** 1993
[22] Monkhorst H J and Pack J D 1976 *Phys. Rev.* B **13** 5188
[23] Yin M T and Cohen M L 1982 *Phys. Rev.* B **26** 5668
[24] Durandurdu M and Drabold D A 2003 *Phys. Rev.* B **67** 212101
[25] Ramachadran G, McMillan P F, Deb S K, Somayazulu M, Grko J, Dong J and Sankey O T 2000 *J. Phys.: Condens. Matter* **12** 4013
[26] Moll N, Bockstedte M, Fuchs M, Pehlke E and Scheffler M 1995 *Phys. Rev.* B **52** 2550
[27] Needs R J and Martin R M 1984 *Phys. Rev.* B **30** R5390
[28] McSkimin H J and Andreatch P Jr 1964 *J. Appl. Phys.* **35** 2161
[29] Hundt R, Schön J C, Hannemann A and Jansen M 1999 *J. Appl. Crystallogr.* **32** 413